

Suzaku Observations of γ -Ray Bright Radio Galaxies: Origin of the X-ray Emission and Broad-Band Modeling

Yasushi Fukazawa^{1,2}, Justin Finke³, Łukasz Stawarz^{4,5}, Yasuyuki Tanaka², Ryosuke Itoh¹, and
Shin'ya Tokuda¹

fukazawa@hep01.hepl.hiroshima-u.ac.jp

ABSTRACT

We performed a systematic X-ray study of eight nearby γ -ray bright radio galaxies with *Suzaku* for understanding the origin of their X-ray emissions. The *Suzaku* spectra for five of those have been presented previously, while the remaining three (M 87, PKS 0625–354, and 3C 78) are presented here for the first time. Based on the Fe-K line strength, X-ray variability, and X-ray power-law photon indices, and using additional information on the [O III] line emission, we argue for a jet origin of the observed X-ray emission in these three sources. We also analyzed five years of *Fermi* Large Area Telescope (LAT) GeV gamma-ray data on PKS 0625–354 and 3C 78 to understand these sources within the blazar picture. We found significant γ -ray variability in the former object. Overall, we note that the *Suzaku* spectra for both PKS 0625–354 and 3C 78 are rather soft, while the LAT spectra are unusually hard when compared with other γ -ray detected low-power (FRI) radio galaxies. We demonstrate that the constructed broad-band spectral energy distributions of PKS 0625–354 and 3C 78 are well described by a one-zone synchrotron/synchrotron self-Compton model. The results of the modeling indicate lower bulk Lorentz factors compared to those typically found in other BL Lac objects, but consistent with the values inferred from modeling other LAT-detected FRI radio galaxies. Interestingly, the modeling also implies very high peak ($\sim 10^{16}$ Hz) synchrotron frequencies in the two analyzed sources, contrary to previously-suggested scenarios for FR I/BL Lac unification. We discuss the implications of our findings in the context of the FRI/BL Lac unification schemes.

¹Department of Physical Science, Hiroshima University, 1-3-1 Kagamiyama, Higashi-Hiroshima, Hiroshima 739-8526, Japan

²Hiroshima Astrophysical Science Center, Hiroshima University, 1-3-1 Kagamiyama, Higashi-Hiroshima, Hiroshima 739-8526, Japan

³U.S. Naval Research Laboratory, Code 7653, 4555 Overlook Ave. SW, Washington, DC, 20375-5352, USA

⁴Institute of Space and Astronautical Science, JAXA, 3-1-1 Yoshinodai, Chuo-ku, Sagami-hara, Kanagawa 252-5210, Japan

⁵Astronomical Observatory, Jagiellonian University, ul. Orla 171, 30-244 Kraków, Poland

Subject headings: radiation mechanisms: non-thermal — galaxies: active — galaxies: individual (PKS 0625–354, 3C 78) — galaxies: jets — gamma rays: galaxies — X-rays: galaxies

1. Introduction

Radio galaxies constitute the parent population of blazars, with low-power radio galaxies thought to be misaligned BL Lacertae objects (BL Lacs), and higher-power sources thought to be associated with flat spectrum radio quasars (FSRQs; e.g., Urry & Padovani 1995). In general, the accretion power determines the radiative properties of the direct emission of the accreting matter (i.e., the thermal continuum of the accretion disk and circumnuclear dust), and is reflected in the presence of high-excitation emission lines in the source spectrum (Hine & Longair 1979). In particular, the “low-excitation radio galaxies” (LERGs) are considered to be characterized by lower accretion rates (below $\sim 1\%$ in the Eddington units) and radiatively inefficient accretion flows, while “high-excitation radio galaxies” (HERGs) are believed to represent high-accretion rate sources with standard (optically-thick, geometrically-thin) accretion disks. The jet power, on the other hand, which in general scales with the total radio luminosity, was proposed to be related uniquely to the large-scale morphologies of radio galaxies (Fanaroff & Riley 1974), with low- and high-power jets forming Fanaroff-Riley (FR) type I and type II structures, respectively. The “FSRQs/FR IIs/HERGs vs. BL Lacs/FR Is/LERGs” unification scenario is not without its caveats, however, as a number of BL Lacs have been found to be associated with FR II-like jets and lobes, while some FSRQs display FR I large-scale morphologies (e.g., Blundell & Rawlings 2001; Heywood et al. 2007; Landt & Bignall 2008; Chiaberge et al. 2009; Kharb et al. 2010). Also, many FR II-type radio galaxies are classified as LERGs, while some FR Is are known to be hosted by high-excitation nuclei (e.g., Hardcastle et al. 2006, 2007, 2009; Buttiglione et al. 2010; Gendre et al. 2013; Mingo et al. 2014).

Studying the core emission of radio galaxies in the aforementioned context of unification schemes for active galactic nuclei (AGN) can be challenging however, due to the inevitable contributions from relativistic jets, host galaxies, accretion disks, and disk coronae, any one of which may dominate the observed radiative output of a source in different frequency ranges. Hence, a detailed multifrequency analysis is needed to disentangle robustly various emission components in a number of objects, before drawing any definite conclusions regarding the corresponding jet and accretion luminosities. We note that although the extended, \geq kpc-scale jets have been resolved in the X-rays and optical for a number of sources¹, sub-kpc scale structures cannot be imaged at

¹See <http://hea-www.harvard.edu/XJET/> and <http://astro.fit.edu/jets/> for continually updated lists of large-scale jets resolved in X-rays and optical, respectively.

frequencies higher than radio, with a few exceptions (see Harris et al. 2009; Goodger et al. 2010; Worrall et al. 2010; Meyer et al. 2013). For this reason, even for the brightest radio galaxies such as Cen A and NGC 1275, the origin of the observed optical and X-ray core fluxes is still an open issue (e.g. Yamazaki et al. 2013). Often, the jet origin of the unresolved core emission is claimed based solely on the modeling of broad-band spectral energy distributions (SEDs; see, e.g., Chiaberge et al. 2003 and Foschini et al. 2005 for the case of NGC 6251), and therefore the alternative possibilities, such as a disk/corona emission, cannot be ruled out.

In the X-ray domain there are three pieces of evidence that can help to distinguish between thermal disk/corona emission and non-thermal radiation from an unresolved jet: variability, the Fe-K line, and — to a lesser extent — the spectral slope. Non-thermal jet emission is expected to be variable on shorter timescales and with greater magnitude than variations in an accretion disk/corona, so fast variability would be an indication of a jet origin, although a lack of such variability would not rule out a jet origin. Variability constraints were used for example in the *Suzaku* study of Cen A by Fukazawa et al. (2011b), who claimed a dominant jet contribution at energies above 100 keV. Yamazaki et al. (2013), on the other hand, concluded that the X-ray core emission from NGC 1275 is dominated by accreting matter due to a large equivalent width (70–120 eV) of the detected Fe-K line. Good constraints on Fe-K lines can be achieved by the *Suzaku* or *XMM-Newton* telescopes, which provide quality X-ray spectra with high signal-to-noise ratios. Obviously, it is possible that in many or even the majority of cases the observed X-ray core emission is a combination of disk/corona and jet contributions, as suggested by the fact that the X-ray spectra of non-jetted AGN are typically harder than those of jetted sources (e.g., Perola et al. 2002); we note however that the spectral slopes of X-ray continua alone do not provide conclusive evidence in this context (see the related discussion in Hardcastle & Worrall 1999). Optical line emission can be also used as an additional constraint to diagnose the disk emission in the objects we study.

During the last decade, rapid developments in γ -ray astronomy has opened a new window for studying the unification of jetted AGN. Blazars are generally bright in the γ -ray band (Hartman et al. 1999; Ackermann et al. 2011) due to relativistic beaming of the jet emission, which is expected to not be as significant for misaligned radio galaxies. Still, recent observations by the *Fermi* Large Area Telescope (LAT) in the high-energy (HE; 0.1 – 100 GeV) band, as well as by the atmospheric Cherenkov telescopes in the very high-energy (VHE; > 0.1 TeV) band, have revealed that radio galaxies are high-energy emitters. In particular, *Fermi*-LAT has detected 11 radio galaxies with 15 months of sky survey data (Abdo et al. 2010b), including M 87 (Abdo et al. 2009b), Cen A (Abdo et al. 2010a), and NGC 1275 (Abdo et al. 2009a). These three objects are also the only established TeV emitting radio galaxies (Aharonian et al. 2006, 2009; Aleksić et al. 2012, respectively), taking into account that the VHE-detected IC 310 (Aleksić et al. 2010) is now proposed to be re-classified as a BL Lac object (Kadler et al. 2012).

Here, we report the *Suzaku* (Mitsuda et al. 2007) X-ray study of eight nearby (redshifts $z < 0.06$) γ -ray emitting radio galaxies which are included in the 15-month *Fermi*-LAT ‘misaligned AGN’ list (Abdo et al. 2010b). All these radio galaxies are of the FRI type, with the exception of

3C 111 and NGC 6251 which display classical FR II and intermediate FR I/FR II large-scale radio morphologies, respectively (e.g., Gliozzi et al. 2004; Sambruna et al. 2004; Grandi et al. 2012). The remaining three radio galaxies from the misaligned AGN sample are all distant ($z > 0.25$) so we do not explore them here. In Section 2 we present our original *Suzaku* data analysis for M 87, PKS 0625–354, and 3C 78; *Suzaku* results for the other sources we discuss, 3C 111, 3C 120, Cen A, NGC 1275, and NGC 6251, are quoted from the literature. In Section 3 we also present the analysis of 5 years of *Fermi*-LAT data for two particularly intriguing sources, PKS 0625–354 and 3C 78. In Section 4 we discuss the origin of the X-ray emission detected with *Suzaku* from unresolved cores of eight analyzed radio galaxies. There we also present for the first time the broad-band SED modeling of PKS 0625–354 and 3C 78 which appear to have X-rays originating from non-thermal jet emission and have not been previously modeled; the modeling is then compared with the analogous modeling of Cen A, NGC 1275, M 87, and NGC 6251 presented previously in the literature. Our main conclusions are summarized in Section 5.

2. *Suzaku* Observations

2.1. Data Reduction

Suzaku is an X-ray observatory which contains two instruments; the X-ray Imaging Spectrometer (XIS; Koyama et al. 2007) and the Hard X-ray Detector (HXD; Takahashi et al. 2007; Kokubun et al. 2007). The former consists of four CCD cameras. One CCD has been lost in 2006 November, and thus most of observational results shown in this paper were based on the data of three CCD cameras. The latter consists of PIN photo-diodes and GSO scintillators, surrounded by active shields of BGO scintillators. All the available *Suzaku* data for the GeV emitting FR I radio galaxies are summarized in Table 1. Results for some of the targets have already been published, as indicated in the table; the *Suzaku* results for M 87, PKS 0625–354, and 3C 78 are presented here for the first time. The Fe-K line equivalent widths and the X-ray luminosities of all the objects provided in Table 1 and discussed in detail below in this paper are estimated by analyzing the archival *Suzaku* data, including the results of Fukazawa et al. (2011a). All the observations were performed in the XIS 5×5 or 3×3 modes, and with the normal mode of the HXD. We utilized data processed with version 2.0–2.7 of the pipeline *Suzaku* software, and performed the standard data reduction: a pointing difference of $< 1.5^\circ$, an elevation angle of $> 5^\circ$ from the earth rim, a geomagnetic cut-off rigidity (COR) of > 6 GV, and > 256 s spent in the South Atlantic Anomaly (SAA). Further selections were applied: Earth elevation angle of $> 20^\circ$ for the XIS, Cut-off-rigidity (COR) > 8 GV and the time elapsed from the SAA (T_SAA_HXD) was selected to be > 500 s for the HXD. The XIS response matrices were created with `xisrmfgen` and `xissimarfgen` (Ishisaki et al. 2007). The XIS detector background spectra were extracted at 4–6 arcmin from the target object and then subtracted. We utilized the HXD responses provided by the HXD team. The “tuned” (LCFIT) HXD background files (Fukazawa et al. 2009) were used, and the good time interval (GTI) was determined by taking the logical “AND” of GTIs among XIS data, HXD data, and HXD back-

Table 1: Summary of *Suzaku* observations of eight LAT-detected FR I radio galaxies

Source	Redshift	ObsID	Date	Exposure*	References [†]
3C 78/NGC 1218	0.029	706013010	2011-08-20	97 ks	this study
3C 84/NGC 1275	0.018	—*	2006–2011	—*	Y13
3C 111	0.049	7050400[1-3]0	2010-09-02,09,14	170 ks	T11
3C 120	0.033	7000010[1-4]0	2006-02,03**	147 ks	K07
PKS 0625–354	0.055	706014010	2011-11-03	110 ks	this study
M 87/3C 274	0.004	801038010	2006-11-29	98 ks	this study
Cen A/NGC 5128	— [†]	100005010,	2005-08-19,	94 ks	M07
		7040180[1-3]0	2009-07-20/08-05/08-14	118 ks	F11b
NGC 6251	0.024	705039010	2010-12-02	87 ks	E11

* XIS-0 exposure.

* Twelve pointings.

** Four pointings.

[†] The assumed distance 3.8 Mpc.

[‡] References: Yamazaki et al. (2013); Tombesi et al. (2011); Kataoka et al. (2007); Markowitz et al. (2007); Fukazawa et al. (2011b); Evans et al. (2011).

ground data. For the XIS and HXD-PIN, the Cosmic X-ray Background (CXB) was added to the background spectrum, assuming the flux and spectra in Boldt (1987), although it was negligible for the HXD-GSO.

For XIS and PIN detectors, the energy ranges of 0.45–10 keV and 17–50 keV, respectively, were used in the fitting. In addition, we ignored the 1.75–1.88 keV energy interval in the XIS spectra to avoid the response uncertainty. The X-ray spectra were binned for least χ -square spectral fitting so that one spectral bin contains more than 20 photons. XIS photons were accumulated within 4 arcmin of the galaxy center, with the XIS-0 and -3 data co-added for PKS 0625–354 and 3C 78. For M 87, the XIS-2 CCD was utilized in the same way as above. Since M 87 is embedded in the bright extended X-ray emission of the Virgo intracluster medium, we took the integration radius as 1 arcmin, and the background spectrum was taken from the 1.5–2.5 arcmin ring, and ignored the HXD-PIN data. Since the GSO signal was not significant in all the analyzed objects, and the resulting upper limits above 40 keV are not constraining, below we do not discuss the GSO data analysis results. A relative normalization between the XIS-F and XIS-B was left free to vary, while that between the XIS and PIN was fixed² to 1.17.

2.2. Results

M 87, PKS 0625–354, and 3C 78 are clearly detected with the XIS below 10 keV; PKS 0625–354 is also detected with HXD-PIN above 10 keV. At first, the obtained *Suzaku* X-ray spectra were

²<http://www.astro.isas.jaxa.jp/suzaku/analysis/hxd/gsoarf2/>

Table 2: Summary of *Suzaku* data spectral fitting

Source	N_{H} 10^{20} cm^{-2}	kT keV	Z Z_{\odot}	$L_{0.5-10 \text{ keV}}$ $10^{42} \text{ erg s}^{-1}$	Γ_{X}	$L_{2-10 \text{ keV}}$ $10^{42} \text{ erg s}^{-1}$	EW eV	$\chi^2/\text{d.o.f}$
(1)	(2)	(3)	(4)	(5)	(6)	(7)	(8)	(9)
M 87	10 \pm 6 (1.9)	1.79 \pm 0.02 2.28 \pm 0.03	1.4 \pm 0.8 1.4 \pm 0.2	13	2.42 \pm 0.03	0.7	< 13	674/572
PKS 0625–354	9 \pm 1 (6.36)	0.24 \pm 0.02	0.3 ^(f)	9.6	2.25 \pm 0.02	49	< 7	640/486
3C 78	14 \pm 2 (9.51)	0.29 \pm 0.04 1.07 \pm 0.06	0.3 ^(f) 0.3 ^(f)	1.0	2.32 \pm 0.04	2.0	< 75	572/567
NGC 6251					1.82 $^{+0.04}_{-0.05}$	2.86	< 66	
3C 111					1.65 \pm 0.02	259	40 \pm 9	
3C 120					1.75 $^{+0.03}_{-0.02}$	100	50 \pm 10	
NGC 1275					1.73 \pm 0.03	7.7	75 \pm 7	
Cen A					1.73 \pm 0.03	10	76 \pm 3	

(1) Source. (2) Absorption column density for **phabs** model; the values in the parentheses are the Galactic values $N_{\text{H,Gal}}$ from Kalberla et al. (2005). (3) Temperature in the **apec** fits. For M 87 and 3C 78, two temperatures are shown in the two **apec** model. (4) Abundance in the **apec** fit (fixed in the cases of PKS 0625–354 and 3C 78). (5) Absorption-corrected **apec** luminosity. (6) Photon index in the PL fit; values for bottom five objects are quoted from the corresponding references in Table 1. (7) Absorption-corrected PL luminosity. (8) Equivalent width of Fe-K line. (9) Goodness of the fit (in the case of M 87 the provided $\chi^2/\text{d.o.f}$ value corresponds to the PL fit to the 3–10 keV range; see section 2.2 for details). Values for bottom five objects in column 7, 8, and 9 are originally derived by us.

fit with a single power-law model (PL) multiplied by the Galactic absorption with the column densities fixed to the corresponding values provided by Kalberla et al. (2005). The spectra of all three objects showed some residuals in the soft X-ray band. These residuals could be due to the thermal emission from the hot interstellar or intracluster medium, and/or absorption columns in excess of the Galactic values. Thus, one or two **apec** thermal plasma models were included in the second step of the fitting procedure, and the absorption column densities were let free. In the cases of PKS 0625–354 and 3C 78 the metal abundance of **apec** was fixed to 0.3 solar, which is typical for galaxy groups (e.g., Fukazawa et al. 2004). In the case of M 87, good photon statistics allowed us to leave the metal abundance free, but because the temperature structure of the M 87 core region is complex (e.g., Matsushita et al. 2002), even a two-temperature **apec** model could not fit the soft X-ray continuum well. Since the detailed investigation of the M 87 temperature structure is beyond the scope of this paper, we simply applied a two-temperature **apec** model to the 0.7–10 keV range, constraining the main thermal plasma parameters; then the resulting **apec** model parameter values were fixed during a **apec** + PL model fit to the 3–10 keV range. Inclusion of the additional thermal components improved the fits, which are summarized in Table 2 and presented in Figure 1.

The plasma temperatures and luminosities derived for PKS 0625–354 and 3C 78 are consistent with those of interstellar and intracluster media found in elliptical galaxies and galaxy groups (e.g., Birzan et al. 2004; Fukazawa et al. 2006; Diehl & Statler 2007). We also checked the archival *Chandra* X-ray data for PKS 0625–354 and confirmed that the X-ray appearance of the source is almost point-like with a faint extended halo due to the host elliptical/poor galaxy cluster Abell 3392.

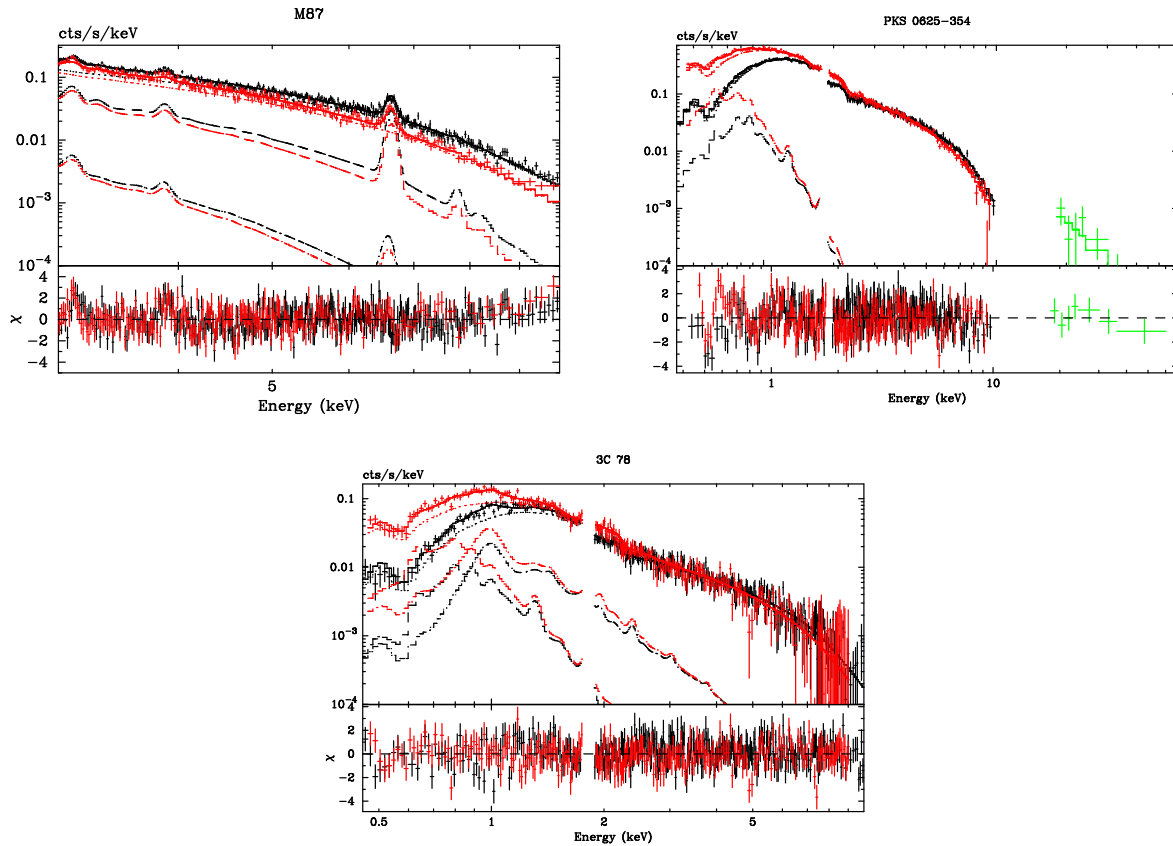


Fig. 1.— *Suzaku* spectra of M87, PKS 0625–354, and 3C 78. The black, red, and green symbols are XIS-F, XIS-B, and HXD-PIN spectra, respectively. The solid line represents the best-fit total model, while the dashed and dotted lines are the *apec* and power-law model components, respectively. We include two *apec* model for M87 and 3C 78. The bottom panels show the residuals in units of σ .

The temperatures of two *apec* components derived for M87 are consistent with those obtained before by Matsushita et al. (2002) based on the analysis of *XMM-Newton* data; the two distinct thermal components in this case are due to the projection of cool-core and hot-periphery cluster emission at the cluster center.

The absorption column densities N_{H} for the three analyzed radio galaxies are slightly larger than the corresponding Galactic value of Kalberla et al. (2005); see Table 2. This might be due to the spectral curvature in the soft X-ray band, but we cannot rule out the uncertainty of the $N_{\text{H,Gal}}$ database, spectral modeling dependency of the thermal emission, and also the intrinsic absorption by the interstellar medium in host galaxies. The derived power-law photon indices Γ_{X} , distributed within a narrow range of 2.22–2.45, are somewhat steeper but not extraordinary for

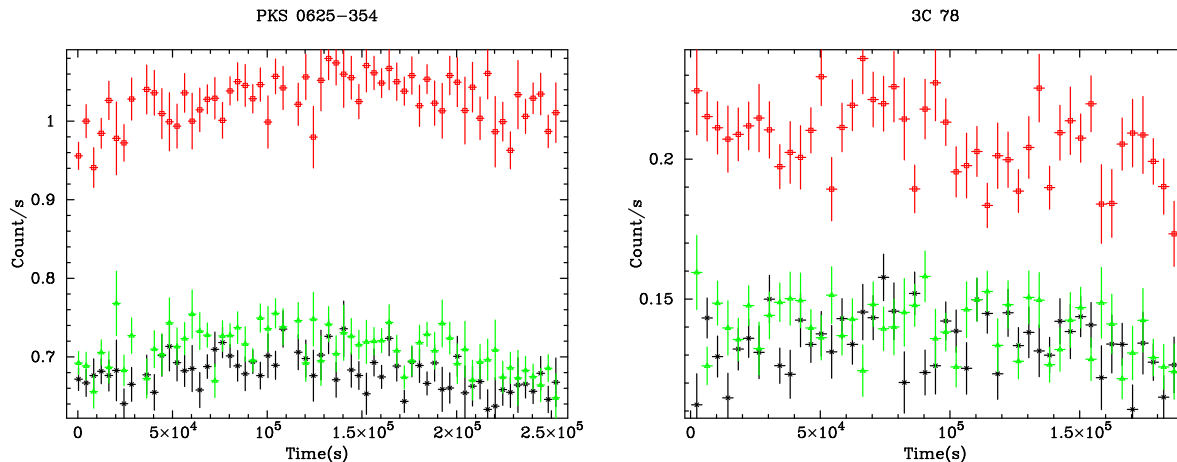


Fig. 2.— *Suzaku* X-ray light curves of PKS0625–354 (left) and 3C 78 (right) in the 0.45–8 keV band. The size of the time bins is 4000 s. The red data points are XIS-B, and others are XIS-F.

coronal emission of Seyfert galaxies. They are also consistent with the X-ray photon indices of high-peaked BL Lac objects (e.g., Donato et al. 2005; Ajello et al. 2009), i.e. the aligned counterpart to FRI radio galaxies, where the X-rays have a jet origin. Fluorescence Fe-K lines are common features in AGNs dominated by disk emission. However, none of the objects analyzed here show significant fluorescence Fe-K lines, except for the ionized Fe-K lines from the hot plasma around the M 87 core. We obtained upper limits of the equivalent widths (EWs) of the narrow Fe-K lines at the rest-frame energy of 6.4 keV (see Table 2); these are particularly low in the cases of PKS0625–354 and M 87.

Glozzi et al. (2008) reported on the 2005 *XMM-Newton* data analysis for PKS0625–354. They found a power-law X-ray component with a photon index of $2.52^{+0.02}_{-0.03}$ and a flux of 2.6×10^{-12} erg cm $^{-2}$ s $^{-1}$; the EW of the Fe-K line was constrained to be < 182 eV. Trussoni et al. (1999) reported on *BeppoSAX* observations of PKS0625–354 and 3C 78 from 1996–1997; assuming a photon index of 2.3 for both sources, they derived the 1–10 keV luminosities of the power-law components as 1.8×10^{43} erg s $^{-1}$ and 1.5×10^{42} erg s $^{-1}$, respectively. Our *Suzaku* observations reveals therefore a flatter-spectrum and brighter (by a factor of 2–3) X-ray emission of PKS0625–354 when compared with the previous epochs. For 3C 78, the X-ray flux is almost the same as that in 1997, and we constrain the power-law photon index and Fe-line EW for the first time. The Fe-K line EWs are in general much more strongly constrained in this study than ever before.

We also investigated the X-ray time variability of the analyzed radio galaxies during the *Suzaku* observations; see Figure 2. No statistically significant variability was found in the 0.45–8 keV range for 3C 78, however most likely only due to a very low photon statistics. PKS0625–354, on the other hand, showed a small amount of variability with a time scale of 1–2 days and an amplitude of $\sim 10\%$. Significant X-ray variability of M 87 detected in the acquired *Suzaku* data will be discussed

(and compared with ongoing *Chandra* monitoring; see Harris et al. 2009) in the forthcoming paper.

3. *Fermi*-LAT Observations

The *Fermi*-LAT is a pair conversion telescope which has a field of view of about 20% of the sky from 20 MeV to over 300 GeV (Atwood et al. 2009). Since our results indicate that the X-ray spectra of PKS 0625–354 and 3C 78 are dominated by jet emission, we analyzed five years of LAT data for those two radio galaxies. As mentioned in Section 1, the SED modeling of M 87 was preformed by Abdo et al. (2009b).

3.1. Data Analysis and Localization

We analyzed the LAT P7REP data from 2008 August 4 to 2013 August 4, corresponding to mission elapsed time (MET) 239557420 to 397353600. Source class (`evclass=2`) events were selected with a zenith angle cut of $<100^\circ$, and a rocking angle cut of 52° . For the analysis, LAT Science Tools version v9r32p5 was utilized with the P7REP_SOURCE_V15 Instrument Response Functions (IRFs). Both radio galaxies are clearly visible in the 0.2 to 300 GeV LAT counts maps. We obtained a localization of the γ -ray sources associated with each galaxy with the `gtfindsrc` task. The resulting localizations were reduced to the 95% confidence localization error $r_{95} = 0.042^\circ$ centered at (RA, DEC) = $(96.785^\circ, -35.488^\circ)$ for PKS 0625–354 (NED: $96.778^\circ, -35.488^\circ$), and $r_{95} = 0.089^\circ$ centered at $(47.145^\circ, 4.130^\circ)$ for 3C 78 (NED: $47.109^\circ, 4.111^\circ$). These localized positions are consistent within 0.007° and 0.046° from the center of the two targets, respectively.

3.2. Results

We extracted the data within a $12 \times 12 \text{ deg}^2$ rectangular region centered on each object. The binned likelihood fitting with the `gtlike` tool was performed. The field background point sources within 14.5° from each source, listed in the LAT 2 year catalog (Nolan et al. 2012), were included, and their spectra were assumed to be power-laws with the photon indices fixed to the catalog values.

Table 3: Summary of the *Fermi*-LAT data spectral fitting

Source (1)	Γ_{HE} (2)	$F_{0.1-100 \text{ GeV}}$ (3)	TS (4)	GBMN (5)	IBMN (6)
PKS 0625–354	1.72 ± 0.06	6.7×10^{-9}	403.2	1.06 ± 0.02	1.38 ± 0.03
3C 78	2.01 ± 0.16	4.9×10^{-9}	61.3	1.04 ± 0.01	0.95 ± 0.03

(1) Source. (2) HE γ -ray photon index. (3) Photon flux in the units of $\text{ph cm}^{-2} \text{ s}^{-1}$. (4) Test Statistics of the detection. (5) Galactic background model normalization. (6) Isotropic background model normalization.

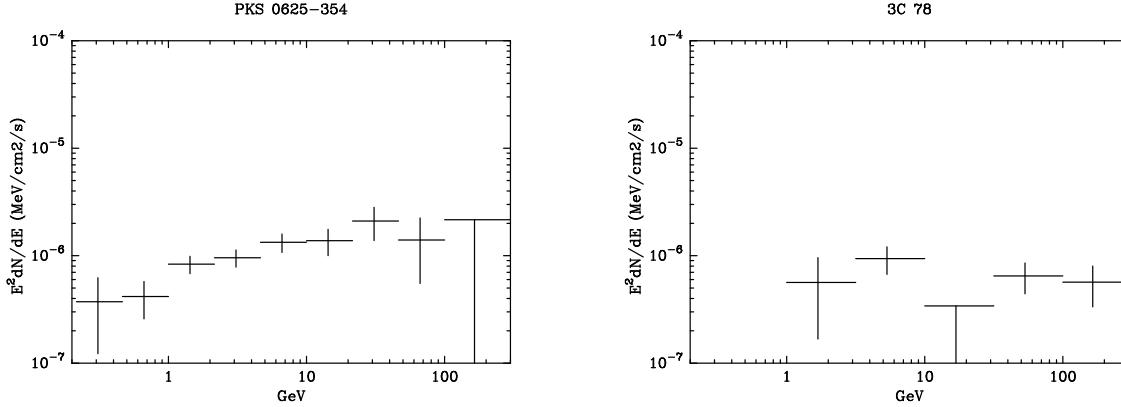


Fig. 3.— *Fermi*-LAT γ -ray spectra of PKS 0625–354 (left) and 3C 78 (right). The data points with only the lower error bar represent upper limits of 90% confidence level flux.

The standard LAT Galactic emission model was used (`gll_iem_v05.fits`) and the isotropic diffuse gamma-ray background and the instrumental residual background were represented as a uniform background (`iso_source_v05.txt`)³. A likelihood analysis was performed with the energy information binned logarithmically in 30 bins in the 0.2–300 GeV band, and the spatial information binned with $0.15 \times 0.15 \text{ deg}^2$ bin size. For the Galactic and isotropic emission models the normalizations were left free. The spectra of both the analyzed radio galaxies were modeled as power-laws.

Table 3 summarizes the *Fermi*-LAT data fitting results. The HE γ -ray photon indices Γ_{HE} (evaluated for the 0.2–300 GeV interval) are within the ‘standard’ blazar range (1.3–3.0) (Abdo et al. 2010d), and we note that PKS 0625–354 and 3C 78 have the hardest LAT spectra among the entire 15 month ‘misaligned AGN’ sample (Abdo et al. 2010b). The values of Γ_{HE} and photon fluxes $F_{0.1-100 \text{ GeV}}$ provided here are in agreement with those given in the 15 month catalog.

In order to obtain model-independent spectra in the 0.2–300 GeV range for our two sources, we performed the `gtlike` spectral analysis for several independent energy bins, which were spaced logarithmically. Nine energy bins were analyzed for PKS 0625–354 and six energy bins for 3C 78. In each energy bin, we fixed the power-law photon index to 2.0. Figure 3 shows the resulting spectra, where we do not detect signals below 1 GeV ($TS < 5$) for 3C 78. Interestingly, the γ -ray detection is significant up to 100 GeV for both objects. In addition, the analysis indicates a break in the γ -ray spectrum of PKS 0625–354. We therefore applied the broken power-law model with `gtlike`, and found that the likelihood L increased by $2\Delta \log L = 401.4$, corresponding to $20\sigma^4$; the

³These background models are available at the FSSC:
<http://fermi.gsfc.nasa.gov/ssc/data/access/lat/BackgroundModels.html>

⁴ $TS=2\Delta \log L$ is distributed as χ^2 for one degree of freedom.

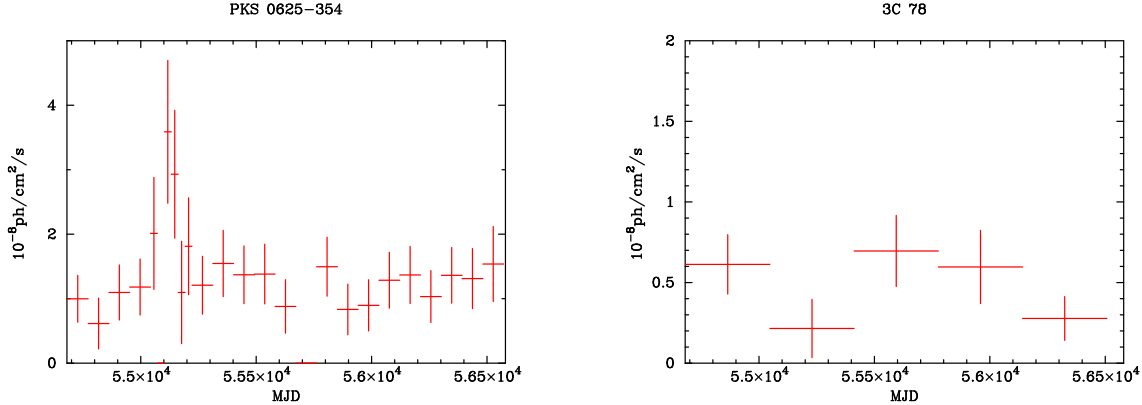


Fig. 4.— *Fermi*-LAT 5-year light curves of PKS0625–354 (left) and 3C 78 (right) in the 0.2–300 GeV range.

resulting photon indices were then derived as 1.69 ± 0.07 and 4.97 ± 1.53 below and above the break energy 64 ± 23 GeV, respectively.

In order to investigate the γ -ray variability of the two analyzed radio galaxies, we binned the LAT data into 30- or 90-day bins for PKS0625–354, and 1-year bins for 3C 78. The `gtlike` analysis was performed for each time bin in the same way as the 5-year analysis of the 0.2–300 GeV band. Figure 4 shows the resulting HE γ -ray light curves. No significant variability can be claimed for 3C 78, but PKS0625–354 displayed a rather pronounced flare during the second year of the LAT operation. Keeping in mind the hardening in the HE γ -ray spectrum of NGC 1275 detected during the flaring state by Kataoka et al. (2010), we split the LAT data for PKS0625–354 into the two 2.5-year long intervals, and performed the `gtlike` analysis for each epoch separately, but we did not find any significant spectral evolution.

4. Discussion

4.1. Origin of the X-ray Emission

In this subsection, we summarize *Suzaku* X-ray studies of the GeV-emitting FR I radio galaxies. Together with the new results on M 87, PKS0625–354, and 3C 78 reported in this paper, we refer to *Suzaku* results from publications listed in Table 1.

For most of the objects in our sample the X-ray spectra are quite similar to those of radio-quiet (non-jetted) Seyfert galaxies, and only in a few cases the power-law photon indices seem somewhat steeper than those typically derived for Seyferts ($\Gamma_X \sim 1.5$ – 2.1 ; e.g., Perola et al. 2002). Therefore,

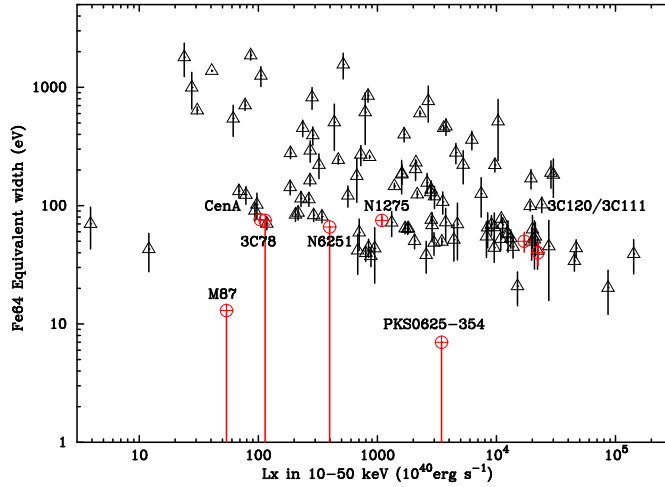


Fig. 5.— Fe-K line EW plotted against the X-ray luminosity for our sample of radio galaxies (red circles) and Seyfert galaxies (black triangles) analyzed by Fukazawa et al. (2011a). The data points with only the lower error bar represent upper limits.

the key feature in distinguishing between the disk/corona versus jet origin for the observed X-ray emission is a fluorescence neutral narrow Fe-K line. This line, commonly observed in Seyfert galaxies accreting at moderate and higher rates with $> 10^{-2} L_{\text{edd}}$, where L_{edd} is the Eddington luminosity, is believed to originate from the Compton-thick dusty torus, which subtends the accretion disk with a large solid angle, as a result of reflection of coronal nuclear X-ray emission. The Fe-K line width and slow variability support the torus origin of a narrow Fe-K line (Fukazawa et al. 2011a). In the case where the X-ray emission is dominated by non-thermal jet radiation, one should not expect a strong Fe-K line, since the jet emission is beamed away from the disk, and so jet photons are not likely to be reflected by the torus. At the same time, sources accreting at particularly low rates with $< 10^{-2} L_{\text{edd}}$ may in principle lack large amounts of circumnuclear dust or prominent coronal components, and as such may be rather weak Fe-K line emitters. Among our sample of targets, four HERGs including Cen A, NGC 1275, 3C 120, and 3C 111 reveal clear Fe-K lines, while the objects classified as LERGs — namely M 87, PKS 0625–354, 3C 78, and NGC 6251 — do not.

Figure 5 shows the Fe-K EW plotted versus the X-ray luminosity L_X (spanning a wide range from $\lesssim 10^{41} \text{ erg s}^{-1}$ up to $\sim 10^{46} \text{ erg s}^{-1}$) obtained with *Suzaku* for Seyfert galaxies, together with our sample of radio galaxies. The Fe-K line-detected radio galaxies are found in the same region of the EW — L_X plane as Seyfert galaxies. Thus, their X-ray emission is likely dominated by disk emission. Other X-ray properties, such as time variability and X-ray relative flux in the SED, also support the disk origin for these sources (Fukazawa et al. 2011b; Yamazaki et al. 2013; Kataoka et al. 2011). However, Cen A is characterized by an excess in hard X-rays (above 100 keV) that smoothly connects to the GeV continuum of the source (Fukazawa et al. 2011b). This may

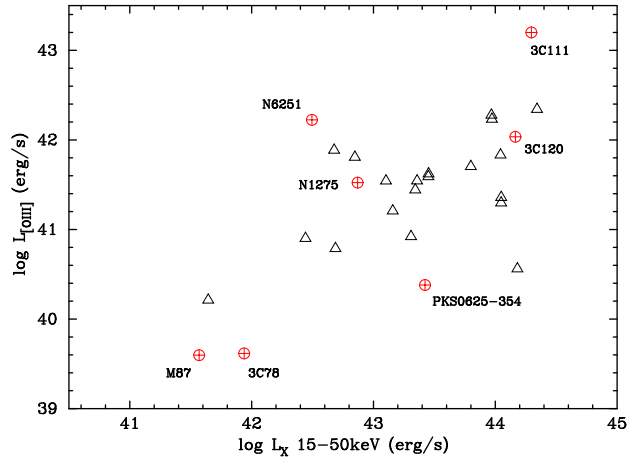


Fig. 6.— Relation between the X-ray luminosity and [O III] 5007Å luminosity for our sample of radio galaxies (filled circles; NED data base) and Seyfert galaxies (empty triangles; data from Mulchaey et al. 1994; Winter et al. 2010).

imply that for this source the X-ray radiation consists of both thermal disk/corona at low energies and non-thermal jet emission at higher energies.

Suzaku puts strong upper limits on the Fe-K line EWs for M 87, PKS 0625–354, and 3C 78. All of these limits are significantly lower than the Fe-K EWs measured for Seyfert galaxies with comparable X-ray luminosities, suggesting that the X-ray emission of these three sources is most likely of jet origin. This, in fact, constitutes the first strong *indication* for compact non-thermal jet emission in the X-ray band for PKS 0625–354 and 3C 78. Note that there is already some evidence that the X-ray emission from the M 87 core is dominated by the jet, albeit different jet regions seem to be pronounced at different activity level of the source (Harris et al. 2009, 2011). One should emphasize however that non-detection of the Fe-K line in a source spectrum does not prove robustly the dominance (or even a presence) of a jet component.

Optical [O III] line emission is also a meaningful indicator of pronounced disk emission, since this line is emitted by the extended gas photoionized by strong disk UV emission. Figure 6 shows a plot of the X-ray luminosity versus [OIII] luminosity. The plot reveals some (weak) hints for a $L_X - L_{[\text{O III}]}$ correlation in the case of Seyferts, but it is not obvious for the analyzed radio galaxies. In particular, the three HERGs in the sample (NGC 1275, 3C 111, and 3C 120) seem to be located in the same region as Seyferts, thus obeying the correlation, while the LERGs seem to be located significantly off the track. This is in agreement with the results of Hardcastle et al. (2009) and Mingo et al. (2014), who showed that the $L_X - L_{[\text{O III}]}$ correlation persists for HERGs, and is not followed by the LERGs in general. This finding can be considered as further support for the scenario for the disk/corona emission dominating the X-ray spectra in “Seyfert-like” sources NGC 1275, 3C 111, and 3C 120, and the jet emission dominating the X-ray output of the outliers

Table 4: Summary of evidence for disk/corona versus jet origin for X-ray emission

Source	Fe-K line	X-ray spectral index	X-ray variability	[O III] line	Type [ref.]
3C 78	jet	jet	inconclusive	jet	LERG [B10]
3C 84	disk/corona	inconclusive	inconclusive	disk/corona	HERG/LERG [†]
3C 111	disk/corona	inconclusive	inconclusive	disk/corona	HERG [‡] [E00]
3C 120	disk/corona	inconclusive	inconclusive	disk/corona	HERG [‡] [E00]
PKS 0625–354	jet	jet	inconclusive	jet	LERG [M14]
M 87	jet	jet	jet	jet	LERG [G13]
Cen A	disk/corona	inconclusive	jet	inconclusive	HERG [E04]
NGC 6251	jet	inconclusive	inconclusive	jet	LERG [E11]

Refs: [B10, E00, M14, G13, E04, E11]Buttiglione et al. (2010); Eracleous et al. (2000); Mingo et al. (2014); Gendre et al. (2013); Evans et al. (2004, 2011).

[†] 3C 84 is diversely classified in the literature; see, e.g., Hardcastle et al. (2009); Buttiglione et al. (2010); Gendre et al. (2013).

[‡] 3C 111 and 3C 120 are archetype examples of Broad-Line Radio Galaxies (BLRGs).

like PKS 0625–354. However, a caveat for this conclusion is that luminosity-luminosity correlations in flux-limited samples may not be real, but only induced by selection effects.

We have summarized the evidence for the disk/corona versus jet origin for our sample, as discussed in this Section, in Table 4.

4.2. X-ray/ γ -ray Connection

The GeV γ -ray emission from radio galaxies could originate from the pc/sub-pc scale jet, where the likely mechanism is synchrotron self-Compton (SSC) or external Compton (EC) scattering of the dust torus or broad-line region emission. It could also originate from EC scattering of CMB photons by electrons in the 100 kpc-scale jets or the radio lobes, as established for Cen A (Abdo et al. 2010b). Somewhat tentative detections of the lobes’ γ -ray emission have been reported also for the intermediate FRI/FR II sources NGC 6251 (Takeuchi et al. 2012) and Cen B (Katsuta et al. 2013), based on the spatial offset between the best-fit position of the γ -ray source and the position of the radio core, or the extension of the γ -ray source aligned to the large-scale radio structure, respectively. The γ -ray emission could not be localized precisely or potentially resolved for 3C 78 or PKS 0625–354, due to the large position errors and a combination of relatively large source distances (when compared with those of Cen A or Cen B) and relatively small sizes of their FRI-type radio structures. The variability of PKS 0625–354 however makes the pc scale origin much more likely for this source, and we favor this interpretation for 3C 78 as well. This also allows us to make a connection between the γ -rays and X-ray emission from PKS 0625–354 and 3C 78, which was established as likely of jet origin in the previous section. We therefore model the broadband SEDs of these two sources in the framework of a standard ‘misaligned blazar’ scenario. We combined the new X-ray and γ -ray data presented above with archival radio, optical, and X-ray data from the NASA Extragalactic Database (NED), *XMM-Newton* optical monitor (OM)

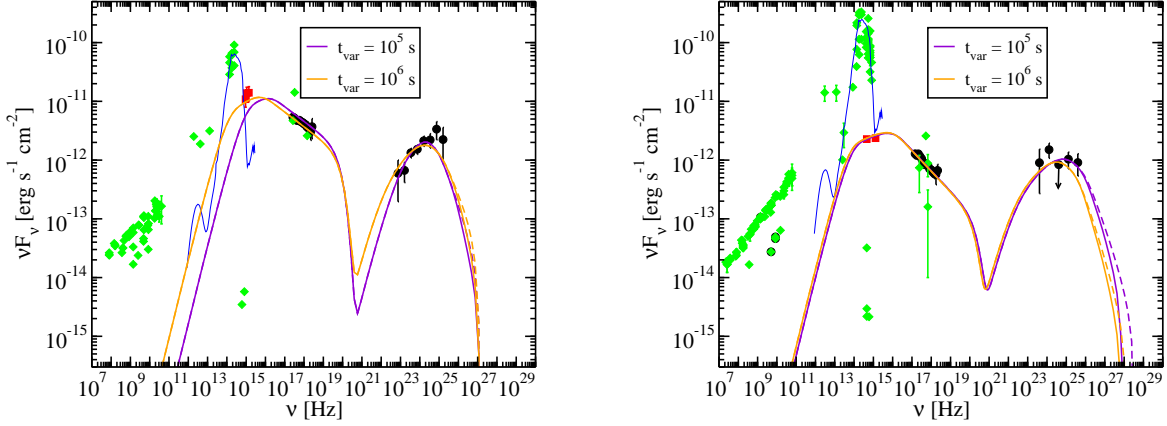


Fig. 7.— SEDs of PKS 0625–354 (left) and 3C 78 (right). Black circles indicate the *Suzaku* X-ray and *Fermi*-LAT γ -ray data presented in this paper, green diamonds are archival data from NED, and red squares are the *XMM-Newton* OM data for PKS 0625–354 (Gliozzi et al. 2008) and core *HST* data for 3C 78 (Chiaberge et al. 2002). The thick curves denote the synchrotron/SSC model fits with two different variability timescales, as given in the legend. The solid curves include $\gamma\gamma$ absorption with the EBL model of Finke et al. (2010), while the dashed curves do not. The thin blue curves are the elliptical galaxy template from Silva et al. (1998), adjusted to the redshifts of the sources.

data from Gliozzi et al. (2008), and *Hubble Space Telescope* data from Chiaberge et al. (2002). The resulting SEDs are presented in Figure 7. It seems fairly clear, looking at the figure, that the nonthermal synchrotron peak in both targets lies between the core optical and X-ray emission, i.e., between 10^{15} and 10^{17} Hz, and we elaborate more on this point further below.

We fit the Gliozzi et al. (2008) and Chiaberge et al. (2002) optical, *Suzaku* X-ray, and LAT γ -ray data assuming they originate as non-thermal synchrotron/SSC from a relativistic jet with the one-zone synchrotron/SSC model from Finke et al. (2008). The resulting model curves are shown in Figure 7 and the model parameters are listed in Table 5. See Finke et al. (2008) for a description of the model parameters and other model details. In our modeling we do not include a component from the disk/corona, consistent with our results from Section 4.1. We also did not fit the radio data, as this is likely to be from a superposition of self-absorbed jet components unrelated to the rest of the SED (Konigl 1981), and as such should be considered as upper limits in our one-zone synchrotron/SSC modeling. The near infrared/integrated optical segments of the broadband spectra are clearly dominated by host galaxies, and therefore in our modeling we added a template of a giant elliptical from Silva et al. (1998), adjusted to the redshifts of the analyzed sources; this template reproduces the optical data well. We assumed a relatively large jet angle to the line of sight (θ in Table 5), consistent with the sources being misaligned BL Lacs, and used two variability timescales to test the robustness with respect to this poorly-constrained parameter. The models

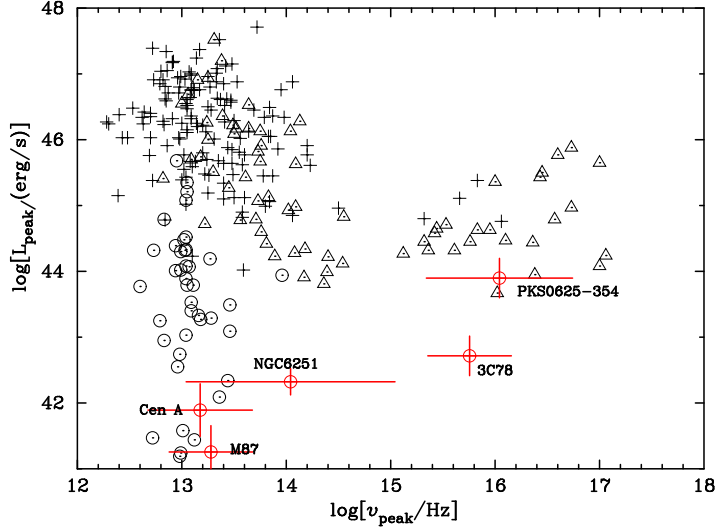


Fig. 8.— Relation between synchrotron peak frequencies and peak luminosities of PKS 0625–354 and 3C 78, together with other sources from our sample of radio galaxies (red circles). For a comparison, radio galaxies, BL Lacs, and FSRQs from Meyer et al. (2011) are also plotted (black circles, triangles, and crosses, respectively).

with two different variability timescales are given in Table 5. Also listed in Table 5 are the results of one-zone synchrotron/SSC models applied to reproduce several other LAT-detected FRI radio galaxies from the literature. Model parameters for PKS 0625–354 and 3C 78 are consistent with those for other radio galaxies which have been modeled previously, as shown in the table. The parameters Γ and δ are lower than typically found in models of BL Lacs. We note that the black hole mass in PKS 0625–354 is estimated to be $10^{9.2} M_{\odot}$ (Bettoni 2003), and in 3C 78 as $10^{8.7} M_{\odot}$ (Rinn et al. 2005); these are the typical values for radio galaxies ($10^{8.1-9.5} M_{\odot}$; McLure et al. 2004) and BL Lac objects ($10^{7.9-9.2} M_{\odot}$; Barth et al. 2003).

One major difference is the models for PKS 0625–354, 3C 78, and NGC 6251 (Migliori et al. 2011) have a higher γ_{brk} by a factor of 10 compared to other radio galaxies in the table. The larger γ_{brk} leads to higher peak synchrotron frequencies and lower electron jet powers compared to magnetic jet powers. For Cen A, M 87, and NGC 1275, the models result in approximate equipartition between magnetic field and electron jet powers. The higher γ_{brk} parameters for PKS 0625–354 and 3C 78 are in turn mainly the result of the harder γ -ray spectra and soft X-ray spectra. Cen A, NGC 6251, M 87, and NGC 1275 have soft LAT spectra ($\Gamma_{HE} > 2.1$), while the LAT spectra for PKS 0625–354 and 3C 78 are harder ($\Gamma_{HE} < 2.1$), although NGC 1275 is a borderline case. As we have already noted above, PKS 0625–354 and 3C 78 were the hardest sources of the *Fermi*-LAT ‘misaligned AGN’ list of Abdo et al. (2010c). The X-ray spectra for Cen A (Abdo et al. 2010a), M 87 (Abdo et al. 2009b), NGC 1275 (Abdo et al. 2009a), and NGC 6251 (Migliori et al. 2011) are hard ($\Gamma_X < 2$), indicating they originate from the SSC component, although M 87 likely has some

synchrotron contribution as well (Abdo et al. 2009b). Assuming jet origin, the soft X-ray spectra ($\Gamma_X > 2$) for PKS 0625–354 and 3C 78 indicates the X-rays originate from synchrotron emission, implying a high peak synchrotron frequency and γ_{brk} .

Meyer et al. (2011) proposed a scenario where low-power jets (BL Lacs and FR I radio galaxies) have longitudinal bulk Lorentz factor gradients. In this scenario, when viewing more aligned jets one observes the faster portion of the outflow resulting in high synchrotron peaked sources, while for progressively more misaligned sources one sees progressively slower portions of the jet and progressively lower synchrotron peak frequencies. Meyer et al. also argued that such gradients are absent in high-power jets (FSRQs and FR II radio galaxies). In Figure 8, we plot the synchrotron peak luminosity (L_{peak}) versus the synchrotron peak frequency (ν_{peak}) for the sample analyzed by Meyer et al. (see Figure 4 therein), along with the results of model fits from the literature and from this paper for γ -ray bright radio galaxies. Error bars on ν_{peak} and L_{peak} were found from visual inspection of the SEDs. We do not include here NGC 1275, since its synchrotron peak is poorly constrained (Abdo et al. 2009a). The sources PKS 0625–354 and 3C 78 are found to have relatively high values of ν_{peak} , not expected in the framework of the scenario of Meyer et al. (2011). This seems to disfavor to some extent their model, which states that high-peaked sources are only the most aligned jets.

It should be emphasized here that the values of ν_{peak} and L_{peak} from Meyer et al. (2011) were found from polynomial fits to radio, optical, and X-ray data, while values derived or adopted by us for γ -ray bright radio galaxies are found from a synchrotron/SSC model fit. Our model fits are more physically-motivated, but also come with additional assumptions. From the point of view of the Lorentz factor gradient scenario, our models are probably preferred, since this scenario assumes synchrotron/SSC emission. 3C 78 is included in the sample of Meyer et al. (2011), but they obtained significantly lower values for ν_{peak} than we did (see their Table 3). We believe this is for two reasons: (i) their phenomenological model fit the radio data, while our synchrotron models do not; and (ii) the inclusion of the hard LAT data spectra require high values of γ_{brk} , which result in high values for ν_{peak} . The latter indicates that LAT observations can be important for modeling the synchrotron portion of a radio loud AGN, even though the γ -rays are not directly produced by synchrotron emission.

Finally, we note there is some ambiguity as to whether PKS 0625–354 is a BL Lac object or a radio galaxy. The optical spectrum of PKS 0625–354 resembles that of a BL Lac (Wills et al. 2004), although its radio morphology resembles an FR I radio galaxy (Ojha et al. 2010). PKS 0625–354 possesses a relatively bright unresolved core (Govoni et al. 2000), as does 3C 78 (Chiaberge et al. 2002), and all the LAT-detected radio galaxies in Table 5. They probably all have intermediate jet alignments, with θ in the range $\sim 10^\circ$ to 30° .

Table 5: SED model parameters of radio galaxies

	PKS 0625–354		3C 78		Cen A	M 87	NGC 1275	NGC 6251
Γ	5.8	5.7	2.93	5.75	7.0	2.3	1.8	2.4
δ	5.8	5.8	2.92	5.75	1.0	3.9	2.5	2.4
θ [deg]	10	19	20	20	30	10	25	25
B [G]	0.82	0.11	0.77	0.02	6.2	0.055	0.05	0.04
t_v [Ms]	0.1	1	0.1	1	0.1	1.2	30	1.7
R_b [10^{16} cm]	1.6	16	0.85	17	0.3	1.4	200	12
p_1	2.5	2.5	2.7	2.7	1.8	1.6	2.1	2.75
p_2	3.5	3.5	3.7	3.7	4.3	3.6	3.1	4.0
γ_{min}	6×10^3	6×10^3	1×10^3	1×10^4	3×10^2	1	8×10^2	250
γ_{max}	2×10^6	6×10^6	2×10^7	2×10^7	1×10^8	1×10^7	4×10^5	4.4×10^5
γ_{brk}	2.9×10^4	4.6×10^4	7.3×10^4	1.4×10^5	8×10^2	4×10^3	9.6×10^2	2.0×10^4
$P_{j,B}$ [10^{42} erg s $^{-1}$]	43	740	0.3	2.5	65	0.02	230	0.4
$P_{j,e}$ [10^{42} erg s $^{-1}$]	2	10	0.6	13	31	7	120	160

The model parameters are as follows: Γ is the bulk Lorentz factor, δ is the Doppler factor, θ is the jet angle, B is the magnetic field, t_v is the variability timescale, and R_b is the comoving blob size scale, p_1 and p_2 are the low-energy and high-energy electron spectral indices, respectively, γ_{min} , γ_{max} , and γ_{brk} are the minimum, maximum, and break electron Lorentz factors, respectively, and $P_{j,B}$ and $P_{j,e}$ are the jet powers in magnetic field and electrons, respectively. Rerefences: Abdo et al. (2010a, for Cen A), Abdo et al. (2009a, for M 87), Abdo et al. (2010b, for NGC 1275), Migliori et al. (2011, for NGC 6251).

5. Conclusions

We have presented *Suzaku* results for nearby *Fermi*-LAT detected low-power radio galaxies, three of which are analyzed here for the first time. Based on the Fe-K and X-ray spectral slope, X-ray variability, and [O III] line strength, we argued for the jet origin of the observed X-ray emission in PKS 0625–354 and 3C 78. This conclusion is in agreement with the optical spectral classification of both AGN as “low-excitation radio galaxies”. We have modeled the broadband SEDs of these two objects including the most recent HE γ -ray spectra following from the analysis of the 5 year accumulation of the LAT data. We found that the bulk Lorentz factors of both sources are typical of those found from modeling the SEDs of FRI radio galaxies, and lower than typically found for BL Lac objects. The peak synchrotron frequencies for PKS 0625–354 and 3C 78 are unusually high for radio galaxies, due to their unusually soft X-ray spectra and unusually hard LAT spectra. This seems at odds with the scenario outlined by Meyer et al. (2011), where high synchrotron peaked objects are the most aligned, and progressively less aligned objects have lower synchrotron peaks. Further studies of PKS 0625–354 with very long baseline interferometry will help to clarify this issue (Müller et al. 2013, Truemstedt et al. in preparation).

The authors thank the anonymous referee for helpful comments that helped to improve the paper, and the *Suzaku* and *Fermi* teams for the operation, calibration, and data processing. Y. F. was supported by JSPS KAKENHI Grant Numbers 2400000401 and 2424401400. L. S. was supported by Polish NSC grant DEC-2012/04/A/ST9/00083.

The *Fermi* LAT Collaboration acknowledges generous ongoing support from a number of agencies and institutes that have supported both the development and the operation of the LAT as well as scientific data analysis. These include the National Aeronautics and Space Administration and the Department of Energy in the United States, the Commissariat à l’Energie Atomique and the Centre National de la Recherche Scientifique / Institut National de Physique Nucléaire et de Physique des Particules in France, the Agenzia Spaziale Italiana and the Istituto Nazionale di Fisica Nucleare in Italy, the Ministry of Education, Culture, Sports, Science and Technology (MEXT), High Energy Accelerator Research Organization (KEK) and Japan Aerospace Exploration Agency (JAXA) in Japan, and the K. A. Wallenberg Foundation, the Swedish Research Council and the Swedish National Space Board in Sweden.

Additional support for science analysis during the operations phase is gratefully acknowledged from the Istituto Nazionale di Astrofisica in Italy and the Centre National d’Études Spatiales in France.

This research has made use of the NASA/IPAC Extragalactic Database (NED) which is operated by the Jet Propulsion Laboratory, California Institute of Technology, under contract with the National Aeronautics and Space Administration.

REFERENCES

- Abdo, A. A., Ackermann, M., Ajello, M., et al. 2009a, *ApJ*, 699, 31
- Abdo, A. A., Ackermann, M., Ajello, M., et al. 2009b, *ApJ*, 707, 55
- Abdo, A. A., Ackermann, M., Ajello, M., et al. 2010a *ApJ*, 719, 1433
- Abdo, A. A., Ackermann, M., Ajello, M., et al. 2010b, *Science*, 328, 725
- Abdo, A. A., Ackermann, M., Ajello, M., et al. 2010c, *ApJ*, 720, 912
- Abdo, A. A., Ackermann, M., Ajello, M., et al. 2010d, *ApJ*, 715, 429
- Ackermann, M., Ajello, M., Allafort, A., et al. 2011, *ApJ*, 743, 171
- Aharonian, F., Akhperjanian, A. G., Bazer-Bachi, A. R., et al. 2006, *Science*, 314, 1424
- Aharonian, F., Akhperjanian, A. G., Anton, G., et al. 2009, *ApJ*, 695, L40
- Ajello, M., Costamante, L., Sambruna, R. M., et al. 2009, *ApJ*, 699, 603
- Aleksić, J., Antonelli, L. A., Antoranz, P., et al. 2010, *ApJ*, 723, L207
- Aleksić, J., Alvarez, E. A., Antonelli, L. A., et al. 2012, *A&A*, 539, L2
- Atwood, W. B., Abdo, A. A., Ackermann, M., et al. 2009, *ApJ*, 697, 1071

- Barth, A. J., Ho, L. C., & Sargent, W. L. W. 2003, *ApJ*, 583, 134
- Best, P. N., & Heckman, T. M. 2012, *MNRAS*, 421, 1569
- Bettoni, D. 2003, *A&A* 399, 869
- Bîrzan, L., Rafferty, D. A., McNamara, B. R., Wise, M. W., & Nulsen, P. E. J. 2004, *ApJ*, 607, 800
- Blundell, K. M., & Rawlings, S. 2001, *ApJ*, 562, L5
- Boldt, E. 1987, *Phys. Rep.*, 146, 215
- Buttiglione, S., Capetti, A., Celotti, A., et al. 2010, *A&A*, 509, A6
- Chiaberge, M., Macchetto, F. D., Sparks, W. B., et al. 2002, *ApJ*, 571, 247
- Chiaberge, M., Gilli, R., Capetti, A., & Macchetto, F. D. 2003, *ApJ*, 597, 166
- Chiaberge, M., Tremblay, G., Capetti, A., et al. 2009, *ApJ*, 696, 1103
- Diehl, S., & Statler, T. S. 2007, *ApJ*, 668, 150
- Donato, D., Sambruna, R. M., & Gliozzi, M. 2005, *A&A*, 433, 1163
- Eracleous, M., Sambruna, R., & Mushotzky, R. F. 2000, *ApJ*, 537, 654
- Evans, D. A., Kraft, R. P., Worrall, D. M., et al. 2004, *ApJ*, 612, 786
- Evans, D. A., Summers, A. C., Hardcastle, M. J., et al. 2011, *ApJ*, 741, L4
- Hine, R. G., & Longair, M. S. 1979, *MNRAS*, 188, 111
- Fanaroff, B. L., & Riley, J. M. 1974, *MNRAS*, 167, 31P
- Finke, J. D., Dermer, C. D., Böttcher, M. 2008, *ApJ*, 686, 181
- Finke, J. D., Razzaque, S., & Dermer, C. D. 2010, *ApJ*, 712, 238
- Foschini, L., Chiaberge, M., Grandi, P., et al. 2005, *A&A*, 433, 515
- Fukazawa, Y., Makishima, K., & Ohashi, T. 2004, *PASJ*, 56, 965
- Fukazawa, Y., Botoya-Nones, J. G., Pu, J., Ohto, A., & Kawano, N. 2006, *ApJ*, 636, 698
- Fukazawa, Y., Mizuno, T., Watanabe, S., et al. 2009, *PASJ*, 61, 17
- Fukazawa, Y., Hiragi, K., Mizuno, M., et al. 2011a, *ApJ*, 727, 19
- Fukazawa, Y., Hiragi, K., Yamazaki, S., et al. 2011b, *ApJ*, 743, 124

- Gendre, M. A., Best, P. N., Wall, J. V., & Ker, L. M. 2013, MNRAS, 430, 3086
- Glozzi, M., Foschini, L., Sambruna, R. M., & Tavecchio, F. 2008, A&A, 478, 723
- Glozzi, M., Sambruna, R. M., Brandt, W. N., Mushotzky, R., & Eracleous, M. 2004, A&A, 413, 139
- Goodger, J. L., Hardcastle, M. J., Croston, J. H., et al. 2010, ApJ, 708, 675
- Govoni, F., Falomo, R., Fasano, G., & Scarpa, R. 2000, A&A, 353, 507
- Grandi, P., Torresi, E., & Stanghellini, C. 2012, ApJ, 751, L3
- Hardcastle, M. J., & Worrall, D. M. 1999, MNRAS, 309, 969
- Hardcastle, M. J., Evans, D. A., & Croston, J. H. 2006, MNRAS, 370, 1893
- Hardcastle, M. J., Evans, D. A., & Croston, J. H. 2007, MNRAS, 376, 1849
- Hardcastle, M. J., Evans, D. A., & Croston, J. H. 2009, MNRAS, 396, 1929
- Harris, D. E., Cheung, C. C., Stawarz, L., Biretta, J. A., & Perlman, E. S. 2009, ApJ, 699, 305
- Harris, D. E., Massaro, F., Cheung, C. C., et al. 2011, ApJ, 743, 177
- Hartman, R. C., Bertsch, D. L., Bloom, S. D., et al. 1999, ApJS, 123, 79
- Heywood, I., Blundell, K. M., & Rawlings, S. 2007, MNRAS, 381, 1093
- Hine, R. G., & Longair, M. S. 1979, MNRAS, 188, 111
- Ishisaki, Y., Maeda, Y., Fujimoto, R., et al. 2007, PASJ, 59, 113
- Kadler, M., Eisenacher, D., Ros, E., et al. 2012, A&A, 538, L1
- Kalberla, P. M. W., Burton, W. B., Hartmann, D., et al. 2005, A&A, 440, 775
- Kataoka, J., Reeves, J. N., Iwasawa, K., et al. 2007, PASJ, 59, 279
- Kataoka, J., Stawarz, L., Cheung, C. C., et al. 2010, ApJ, 715, 554
- Kataoka, J., Stawarz, L., Takahashi, Y., et al. 2011, ApJ, 740, 29
- Katsuta, J., Tanaka, Y. T., Stawarz, L., et al. 2013, A&A, 550, A66
- Kharb, P., Lister, M. L., & Cooper, N. J. 2010, ApJ, 710, 764
- Kokubun, M., Makishima, K., Takahashi, T., et al. 2007, PASJ, 59, 53
- Konigl, A. 1981, ApJ, 243, 700

- Koyama, K., Tsunemi, H., Dotani, T., et al. 2007, PASJ, 59, 23
- Landt, H., & Bignall, H. E. 2008, MNRAS, 391, 967
- Markowitz, A., Takahashi, T., Watanabe, S., et al. 2007, ApJ, 665, 209
- Matsushita, K., Belsole, E., Finoguenov, A., Böhringer, H. 2002, A&A, 386, 77
- McLure, R. J., Willott, C. J., Jarvis, M. J., et al. 2004, MNRAS, 351, 347
- Meyer, E. T., Fossati, G., Georganopoulos, M., & Lister, M. L. 2011, ApJ, 740, 98
- Meyer, E. T., Sparks, W. B., Biretta, J. A., et al. 2013, ApJ, 774, L21
- Migliori, G., Grandi, P., Torresi, E., et al. 2011, A&A, 533, A72
- Mingo, B., Hardcastle, M. J., Croston, J. H., et al. 2014, MNRAS, 440, 269
- Mitsuda, K., Bautz, M., Inoue, H., et al. 2007, PASJ, 59, 1
- Mulchaey, J. S., Koratkar, A., Ward, M. J., et al. 1994, ApJ, 436, 586
- Müller, C., Krauss, F., Kadler, M., et al. 2013, arXiv:1301.4384
- Nolan, P. L., Abdo, A. A., Ackermann, M., et al. 2012, ApJS, 199, 31
- Ojha, R., Kadler, M., Böck, M., et al. 2010, A&A, 519, A45
- Perola, G. C., Matt, G., Cappi, M., et al. 2002, A&A, 389, 802
- Rinn, A. S., Sambruna, R. M., & Gliozzi, M. 2005, ApJ, 621, 167
- Sambruna, R. M., Gliozzi, M., Donato, D., et al. 2004, A&A, 414, 885
- Silva, L., Granato, G. L., Bressan, A., & Danese, L. 1998, ApJ, 509, 103
- Takahashi, T., Abe, K., Endo, M., et al. 2007, PASJ, 59, 35
- Takeuchi, Y., Kataoka, J., Stawarz, L., et al. 2012, ApJ, 749, 66
- Tombesi, F., Sambruna, R. M., Reeves, J. N., Reynolds, C. S., & Braitto, V. 2011, MNRAS, 418, L89
- Trussoni, E., Vagnetti, F., Massaglia, S., et al. 1999, A&A, 348, 437
- Urry, C. M., & Padovani, P. 1995, PASP, 107, 803
- Wills, K. A., Morganti, R., Tadhunter, C. N., Robinson, T. G., & Villar-Martin, M. 2004, MNRAS, 347, 771

Winter, L. M., Lewis, K. T., Koss, M., et al. 2010, *ApJ*, 710, 503

Worrall, D. M., Birkinshaw, M., O’Sullivan, E., et al. 2010, *MNRAS*, 408, 701

Yamazaki, S., Fukazawa, Y., Sasada, M., et al. 2013, *PASJ*, 65, 30